Hindawi
Journal of Nanotechnology
Volume 2023, Article ID 3152014, 12 pages
https://doi.org/10.1155/2023/3152014

Research Article

Angular Dependence of Magnetization Behavior in $Ni_{81}Fe_{19}$ Nanowires by Micromagnetic Simulations

Musaab Salman Sultan

Department of Networks and Information Security, Technical College of Informatics, University of Akre for Applied Sciences, Kurdistan, Iraq

Correspondence should be addressed to Musaab Salman Sultan; mussab_ahmmad@yahoo.com

Received 31 July 2023; Revised 30 August 2023; Accepted 9 September 2023; Published 16 October 2023

Academic Editor: Mozhgan Afshari

Nickel (Ni)-iron (Fe) alloy in the form of $Ni_{81}Fe_{19}$ (permalloy) is a widely used material in technological soft magnetic applications. Understanding the magnetization behavior in detail in such materials is substantial from both a scientific point of view and industrial demands. Therefore, the main purpose of the present article is to discuss the angular dependence of magnetization in $Ni_{81}Fe_{19}$ nanowires by micromagnetic simulation using the object-oriented micromagnetic framework (OOMMF) platform. These investigations have been implemented on different widths/thicknesses (T) up to 150 nm with an identical stretch of 1 μm. There was a reduction in the remanent magnetization by increasing the wire angle with respect to the magnetic field applied, which displayed excellent agreement with calculations performed theoretically. This was designated for the effect of shape anisotropy on behavior. The angular dependence of the switching behavior was analyzed and compared theoretically with the classical domain wall reversal models. The magnetic reversal for wires ≤30 nm was well defined by the uniform rotation of the Stoner–Wohlfarth model, whereas for nanostructures ≥50 nm was analyzed by the nonuniform rotation of the curling model. The critical thickness for the transition between these models was theoretically calculated and found to be around 30 ± 5 nm, which is in good agreement with the other findings presented in the literature using other materials of ferromagnetic wires. The micromagnetic spin structure was obtained instantaneously before and after switching events for relatively thick (150 nm) nanostructures at different angles, suggesting that the reversal is not as simple as predicted by the domain wall reversal of nonuniform rotation of the curling model.

1. Introduction

Theoretical and experimental research studies on the magnetization behavior of circular (cylindrical) or rectangular (planar) cross-sectional ferromagnetic nanowires have become increasingly important during the past four decades due to their fascinating configurations that are not realized in three-dimensional materials and present importance in prospective industrial applications, as well as to explore the details of nanotechnology [1–12]. Different ferromagnetic materials have been analyzed, including nickel, iron, cobalt, and some rare earth elements (scandium, yttrium, gadolinium, neodymium, and samarium), as well as their alloys. As an example, $Ni_{81}Fe_{19}$ has attractive magnetic properties, such as high permeability with low coercivity, low eddy-current loss, and low magnetic hysteresis loss, as well as low or even zero magnetostriction and low magnetocrystalline anisotropy [9–12]. This alloy also has a significant anisotropic magnetoresistive effect. These properties, for instance, make permalloy materials widely used in inductance coils, electrical transformers, magnetic shielding, and memory devices, as well as in some magnetic recording media [2–5, 9–12].

The origin of the magnetic state within such ferromagnetic materials, however, arises from the alignments of internal neighboring electron spins, which are strongly dependent on the quantum mechanical exchange interaction. As it is well known from the Pauli Exclusion Principle, any two electrons cannot occupy the same orbital if they have the same quantum numbers [13, 14]. Thus,

repulsive or attractive energy appears when the electron spins are parallel or antiparallel, respectively. Thus, there is electrostatic energy between the nearest neighboring electrons, known as exchange energy or force. This energy, however, is not the only energy responsible for the overall magnetic state within such ferromagnetic materials due to the anisotropic energies arising from different origins that compete with each other to give the overall magnetic state within these materials. There are two main sources of magnetic anisotropy. The first is due to the spin-orbit coupling, including magnetoelastic and magnetocrystalline anisotropies [15, 16]. The second class is termed magnetostatic or shape anisotropy, which is the most significant anisotropy in measuring ferromagnetic nanostructures and is related to dipole-dipole interactions. These anisotropies strongly influence the overall magnetic state of ferromagnetic nanomaterials.

From an experimental point of view, different methods are utilized for producing ferromagnetic nanostructures. The first is the electrodeposition of magnetic elements from chemical solutions to nanoporous templates [17–21]. Using this method, two-dimensional arrays of circular-shaped nanowires or nanotubes can be formed. The other essential methods that have been widely used are lithography and liftoff techniques [5, 22, 23], focused ion/electron beam milling (FIB/FEB) [24], ion/electron-beam-induced deposition (IBID/EBID) [25–27], and atomic/magnetic force microscopy (AFM/MFM) [28, 29]. These procedures, however, fabricate rectangular-shaped nanostructures lying on the substrate parallel to its surface plane [5, 22–29].

The magnetic properties of ferromagnetic nanostructures have been experimentally discovered using a wide range of characterization systems, including alternating gradient magnetometer (AGM), vibrating sample magnetometer (VSM), torque magnetometry (TM), superconducting quantum interference device (SQID), and atomic/magnetic force microscopy [17–23]. On the other hand, the magnetization behavior of isolated (individual) nanowires has been analyzed using micro-SQUID, electro-magneto-transport measurements [30–36], and magneto-optical Kerr effect (MOKE) magnetometry [37–42].

With the modern progress in computing technology and their programming applications, it has become encouraging to utilize micromagnetic simulation to theoretically explore the magnetic properties and explain experimental observations or predict new experimental designs of an extensive variety of ferromagnetic nanostructures, including nanowires [43–51], nanodots, and nanotubes [52–54]. The most widely used micromagnetic simulation software is the OOMMF package. This is because the OOMMF package has the capability to show magnetic hysteresis loops and visualize the magnetic moment at any period throughout a hysteresis loop cycle. These studies, however, have shown that magnetization reversal in ultrathin nanostructures can happen uniformly via coherent rotation, in which all the spins rotate immediately upon applying an external magnetic field [44]. In thicker nanostructures (<100 nm), two unlike models have been described, known as vortex and transverse wall modes [44, 45, 50]. During the submission of an external magnetic field, a reversed domain can nucleate at the ends of the nanostructure or at imperfections [45, 55] separated from the old domain by a newly formed domain wall. Consequential propagation of the domain walls throughout the nanostructure leads to the nanowire switching from one magnetic configuration to another and decreasing the magnetostatic energy. The nucleation at these sites, however, is due to the large demagnetizing field at these places [45]. The magnetic moments precede a spiral motion as the wall spreads parallel to the wire's long axis because of the torque employed on the magnetic spins. The transition between transverse and vortex modes was discussed elsewhere [50] and was found to depend on various elements, including element composition, dimensions, crystalline structure, and surface morphology of the nanostructures, as well as the preliminary magnetic field applied [50].

Nevertheless, most of these studies concentrated on a small number of two-dimensional arrays of nanowires or individual nanowires of smaller diameter/thickness in which the magnetization structures show a simple magnetic state compared to the thick isolated nanostructures, which support more sophisticated reversal behavior. Thus, the magnetization reversal of relatively thick individual nanowires is still confusing and needs more examination. Therefore, the aim of the work presented here is to perform OOMMF modeling to discuss the angular dependence of magnetization behavior in $Ni_{81}Fe_{19}$ nanowires with different T up to 150 nm. The findings were then investigated and compared with the literature and theoretical models of domain wall reversal.

2. Methodology

The OOMMF software was utilized here to explore the magnetic properties of permalloy wires. This package is public domain software available freely from the National Institute of Standards and Technology (NIST) website [56]. It is a group of programs working together to analyze magnetic problems, and each program can be modified or redesigned without varying the entire OOMMF software. The OOMMF code has a good magnetic output file that can display the magnetic state of a simulated sample in different formats, such as data tables, graphs, or magnetic configurations [56–60]. It can also easily calculate the magnetic state dynamics for any arbitrarily shaped material composed of one or more different ferromagnetic elements. The T of permalloy nanowires was chosen to be 10–150 nm with a permanent stretch of 1 μm. This stretch was designated in accordance with the space accessible in the memory and the time required for computation [61].

In the OOMMF platform, it is essential to describe the micromagnetic problem under discussion, which contains nanowires' geometrical shape and dimensions as well as cell size, magnetocrystalline anisotropy, magnetostriction anisotropy, and magnetic considerations for which the calculation is executed. For simplification in the micromagnetic analysis, some of the magnetic anisotropy terms can be neglected depending upon the magnetic system in use.

Thus, micromagnetic simulations were performed by allocating a rectangular piece divided into three-dimensional arrays of cubic cells, as shown in Figure 1. The cell size should be less than or equal to the exchange length to permit the exchange interaction to be appropriately performed [15, 57–59] and to give more accurate and reliable results. Exchange length is of primary importance because it governs the length of the transition between magnetic domains [62].

If the cell size is larger than the exchange length, the simulation would not have enough cells to do a realistic simulation, whereas if the cell size is much smaller than the exchange length, then it slows down the computation speed without any additional gains. Thus, the cell dimensions were chosen to be less than the exchange length (5.3 nm [62]) of permalloy: $2 \times 2 \times 2\,\text{nm}^3$ and $5 \times 5 \times 5\,\text{nm}^3$ for nanowires <50 nm and ≥50 nm, respectively. The magnetic configuration was supposed to be fixed and positioned at the center of each cell.

The factors of exchange stiffness and the saturation magnetic field were nominated to be 13×10^{-12} J/m and 8.6×10^5 A/m, respectively [15, 62]. The magnetostriction energy and magnetocrystalline anisotropy were ignored from the micromagnetic simulation because the magnetostriction energy is very small and adjacent to zero, and permalloy has no magnetocrystalline anisotropy [13–15]. The gyromagnetic ratio defined as default in the OOMMF platform was equal to 17.59 MHz/Oe. Further details can be found elsewhere [15, 43].

The integration of the Landau–Lifshitz–Gilbert (LLG) equation, Runge–Kutta evolver was performed, in which the application of magnetic field was accomplished in steps to achieve energy minimization for each field step. The damping factor was responsible for reducing the energy of the system under discussion. Accordingly, an appropriate stopping condition (1×10^{-5} A/m), which is specified by the torque $M \times H$, was defined in the micromagnetic input file to permit the simulation to finish or progress to the consequent field step [63]. If the stopping step is very low, the simulation will remain for longer periods without any progress. If it is used very high, the simulation will not minimize the energy state, and the results will not be accurate. Thus, to decrease the time of micromagnetic simulation, the damping parameter was taken to be ~0.5, and the stopping step used was dM_dt 1. The field steps and the extreme magnetic field were selected according to initial simulations executed to estimate the shape of the loop. In complete micromagnetic simulations, the field strength was reduced from saturation to the negative sign in steps of 5–10 Oe. Comprehensive information on the micromagnetic simulation and the OOMMF code can be found in the studies in [57–59, 63–65].

In order to gain a full understanding of the magnetic properties and the mechanism of the magnetization reversal in such nanowires, a series of micromagnetic simulations were performed by applying two orthogonal magnetic fields to these nanowires. When the field is applied parallel to the nanowire's long axis, the magnetic moments return through the nucleation and propagation of the walls of the domain. Whereas when the field is applied orthogonally to the nanowire's long axis, the magnetic moments return by pseudocoherent rotation. The results of this investigation may provide a guide to control the magnetic properties of such nanowires for potential technological applications. Thus, the first was applied parallel to the nanowires' long axis (H_x), and the other was applied orthogonally to the nanostructures' long axis (H_y), as presented in Figure 2. Using mathematical equations, the vector sum of the magnetization field along the designated angle β with respect to the nanowire long axis was calculated using the following equation [63]:

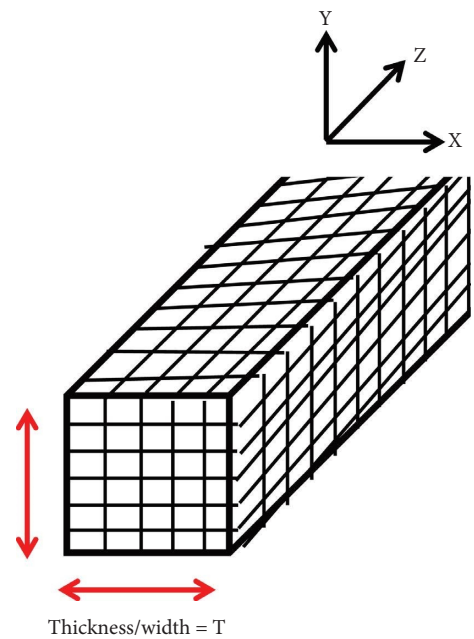

Figure 1: Permalloy wires were produced using rectangular sections divided into three-dimensional arrays of cubic cells. The cell sizes are $2 \times 2 \times 2\,\text{nm}^3$ and $5 \times 5 \times 5\,\text{nm}^3$ for nanowires <50 nm and ≥50 nm, respectively. The thickness/width marked in the figure is denoted as T throughout this article.

$$H_\beta = \sqrt{\left(H_x^2 + H_y^2\right)}. \tag{1}$$

With respect to the magnetic field H_β, the magnetization will change to a net state of M_α. The component of M_α, called M_β, along H_β, can be determined, and the angle $\propto$ can be calculated using the following equation:

$$\tan\alpha = \frac{M_y}{M_x}. \tag{2}$$

The magnetization along the angles α and β is acquired using the following relations:

$$M_\alpha = \sqrt{\left(M_x^2 + M_y^2\right)}, \tag{3}$$

$$M_\beta = M_\phi \cos(\beta - \propto). \tag{4}$$

Thus, the magnetic field H_β was identified in the micromagnetic input file (MIF) to simulate the magnetic hysteresis loops at various wire angles with respect to the

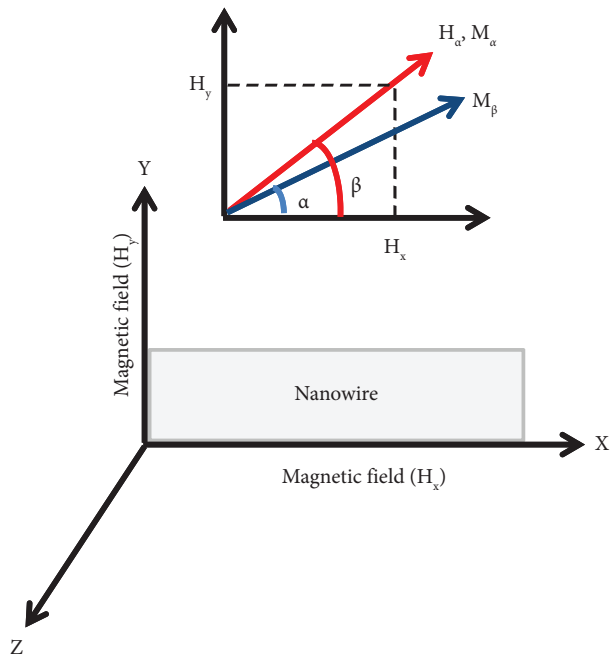

Figure 2: Schematic diagrams presenting the permalloy wire with the coordinate system. Two perpendicular magnetic fields were applied parallel (H_x) and orthogonal (H_y) to the nanowire's long axis with the projections of their components of magnetization. The determined magnetic field at any angle was then defined within the OOMMF platform to examine the angular dependence of the remanent magnetization and switching fields [63].

field applied. Accordingly, the hysteresis loops and the angular dependence of remanent magnetization (M_β) and switching fields (H_β) were determined using equations (1)–(4). The remanent magnetization M_R, at any angle β, can be found by the projection of magnetization towards the measurement direction using the following equation [21]:

$$M_R(\beta) = M_R(\|)|\cos\beta|, \tag{5}$$

where $M_R(\|)$ is the remanent magnetization; at $\beta = 0$, the external magnetic field H_β is with the nanowire long axis.

To theoretically calculate the critical thickness, the switching field for the Stoner–Wohlfarth model, and the curling models for an infinite cylinder, the following equations were utilized [30, 31, 35, 41, 63]:

$$H_{SW} = \frac{M}{2}\frac{b(1+b)}{\sqrt{b^2 + (1+2b)\cos^2\beta_o}} \text{For curling model,} \tag{6}$$

$$H_{SW} = \frac{M}{2}\frac{b}{\left(\sin^{(2/3)}\beta_o + \cos^{(2/3)}\beta_o\right)^{(3/2)}} \text{For Stoner} - \text{Wohlforth model,} \tag{7}$$

$$h_{sw} = \frac{H_{sw}}{2\pi M}, \tag{8}$$

$$b = -1.08\left(\frac{t_0}{t}\right)^2, \tag{9}$$

where β_o is the angle between the externally applied magnetic field and the nanowire's long axis, M is the saturation magnetization of permalloy, and h_{sw}, is the reduced switching field. t and t_o are the thickness/width of the nanowire and the exchange length, respectively. The t_o/t is known as the reduced radius R. The exchange length is given by the following equation [62, 63]:

$$t_o = \frac{E^{1/2}}{M}, \tag{10}$$

where E is the exchange constant, which is dependent on the critical size of the nanowires and independent on the shape and real size of the considerable wires [36, 41].

3. Results and Discussion

The normalized magnetic hysteresis loops of angular dependent of permalloy wires with various T (30 nm, 50 nm, 75 nm, 100 nm, and 150 nm) at different nanowire long axis angles (1°, 15°, 30°, 45°, 60°, 75°, and 90°) with respect to the magnetic field applied externally are shown in Figure 3.

From all measurements examined here, the magnetic loops have a distinct switching behavior. For all T, the magnetic loops have a lower squareness ratio (shared loops in the field) by increasing the nanowire T and angle.

The remanent magnetization against nanowires' long axis angle for various T of nanowires is displayed in Figure 4. Clearly, for all T of wires investigated here, the remanent magnetization is at its maximum when the magnetic field is parallel to the nanowire's long axis. Then, it decreased constantly by increasing the wire angle and disappeared for a magnetic field at an angle of 90°. Comparing this result with the theoretical predictions using relation 5 presented in the methodology section, an excellent agreement was obtained, as established by the fitting dashed lines presented in Figure 4.

For each angle of investigation and for nanowires with T up to 100 nm, the remanent magnetization is nearly close to each other and is higher than 150 nm thick nanowires. At high angles of measurement (≥75°), the remanent magnetization values are almost the same for all T of wires, and they are at minimum values. For all of the angles discussed here, a reduction in the remanent magnetization was noticed with increasing nanowire T, and this was analyzed in detail in other research studies [43, 63, 66]. However, the reduction in remanent magnetization with increasing nanowire T was attributed to the formation of multidomain structures or moment rotations within the magnetic structure due to the effect of the magnetostatic anisotropy and demagnetizing field, which increases with increasing nanowire thickness.

Now, the drop in the remanent magnetization with increasing nanowires angle can be described as follows: when the nanostructure's long axis is parallel to the external magnetic field, H_β, the remanence ratio, as predicted, reveals the maximum value in all of the thicknesses of wires explored here. This is due to the shape anisotropy because the magnetic spins are primarily directed along the easy axis of magnetization.

Upon increasing the wire's angle and removing this field, the magnetic spins relax and are redirected again parallel to the nanowire's long axis. As a result, the remanent magnetization is decreasing in that direction with an increase in the nanowire angles. This behavior is more remarkable in relatively thick nanowire (150 nm) due to the reduction of the shape anisotropy with increasing nanowire T and the effect of the demagnetizing field.

Returning to Figures 3(d)–3(e) and their insets, clearly, the loop shapes are complicated and exhibit various switching structures with increasing the wire angle, not as predicted by the curling model of domain reversal [13–15]. This complication in the switching events might be due to the formation of complex multidomain structures upon increasing the wire's long axis angle with respect to the magnetic field applied.

To understand the complexity behavior in the switching events of relatively thick wires, an example of micromagnetic moment distributions for the 150 nm thick nanowires obtained during the switching states at several angles is shown in Figure 5. The color variation represents the magnitude along a certain direction, such as the x-y and x-z angles of the magnetic spin. These micromagnetic spin structures were obtained instantaneously from energy-minimized states at two different field steps before and after the switching events and are shown as an axial portion over the center of such wires. These snapshots reveal the complexity in the configuration of magnetic spins throughout the switching, which may also indicate that the magnetization reversal in such relatively thick wires is not as simple as in the curling-like behavior, as will be discussed in the subsequent investigations.

To investigate the magnetization reversal in detail in such nanowires, the switching fields were extracted from the hysteresis loops and plotted against the nanowire's long axis angle, as shown in Figure 6. Two regimes were recognized for nanowires with T ≤30 nm; strong reduction in the switching field was observed with an increase in the wire angle up to 20°. Between 20° and 60°, the switching field is approximately fixed. Then, the switching field increases quickly at greater nanowire angles (~60°). A similar trend was noticed with nanowires of thickness 10 nm but with greater values of switching fields in all angles studied here (not shown in the figure due to their large values of switching fields). In contrary, for nanostructures with T higher than 50 nm, it is increasing gradually up to ~40°, and then increasing quickly to the highest value. This result indicates that there is a transition in the magnetization behavior between nanowires of 30 nm and 50 nm thicknesses. This finding is in excellent agreement with the other findings investigated in the literature using other materials for ferromagnetic wires and the same and other characterization methods [35, 36, 45].

As an example, the critical thickness, t_o, for the transition of transverse to vortex wall modes of Fe and Ni wires was established to be 20 nm and 40 nm, respectively, as calculated using micromagnetic modeling on cone cross-sectioned Fe and Ni wires [45]. Nonetheless, this is close to 34 ± 4 nm obtained experimentally from electrodeposited Ni nanowires using micro-SQUID and was attributed to the transition between uniform and nonuniform modes of reversal [35, 36].

The critical thickness of the nanowires considered here was calculated using the relations (6)–(10) presented in the methodology section and was found to be around 30 ± 5 nm, which is in full agreement with the finding stated above and reported in the literature [35, 36].

Finally, for all angles investigated here, there was a reduction in the switching fields with increasing nanowires T. The reduction in the switching fields with increasing

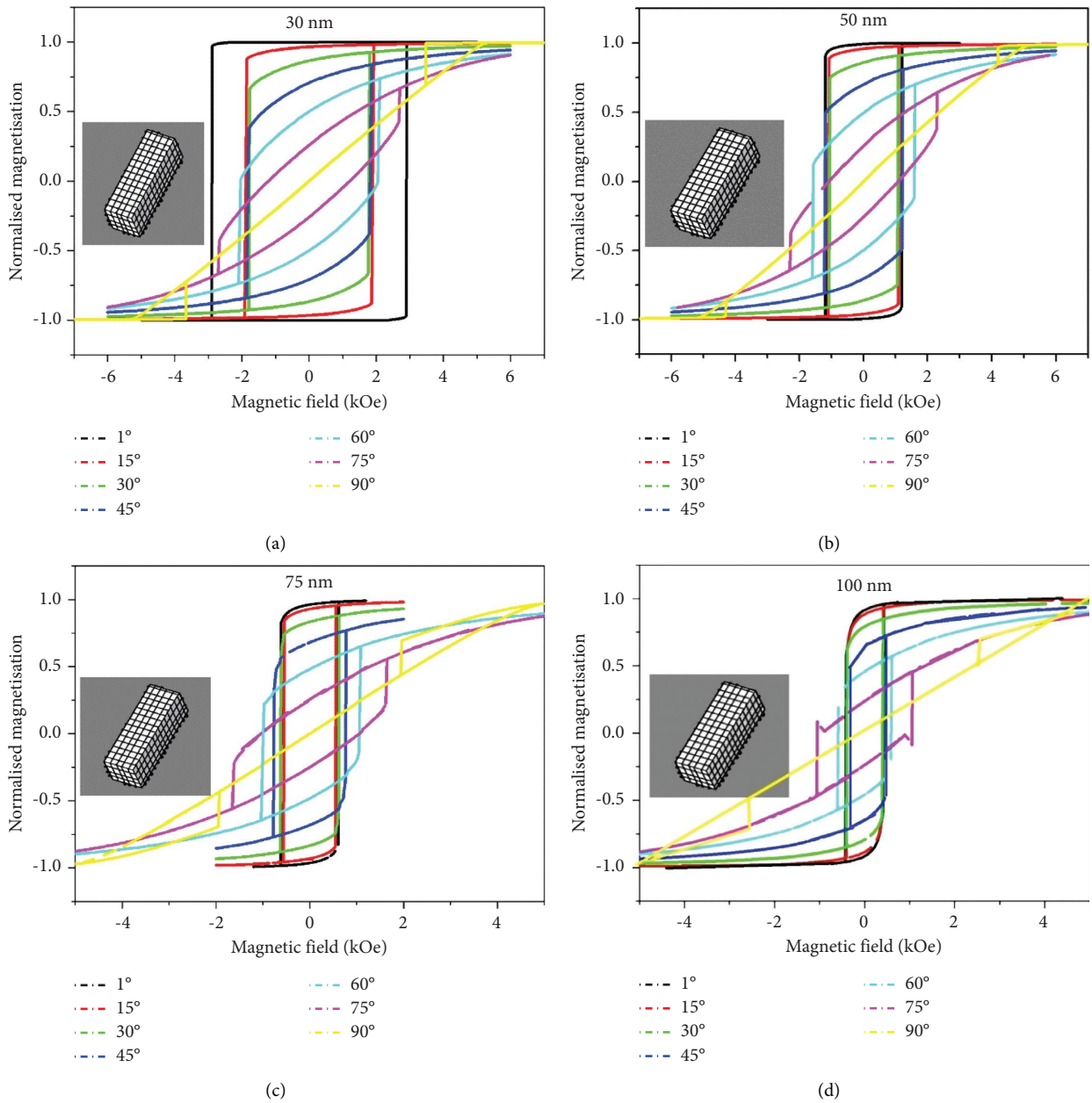

Figure 3: Continued.

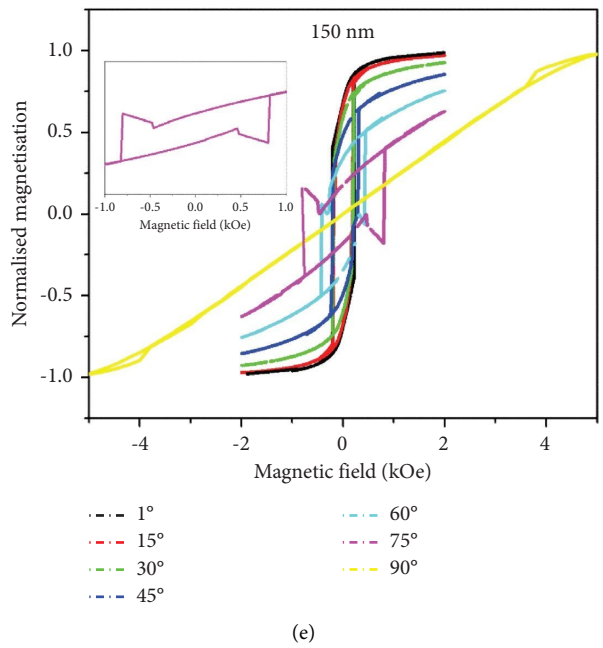

Figure 3: Normalized loops acquired from the simulations of $Ni_{81}Fe_{19}$ wires with different T at various wire angles with respect to the field applied, as specified in the loop titles. Note the difference in the magnetic field scale bars of the hysteresis loops.

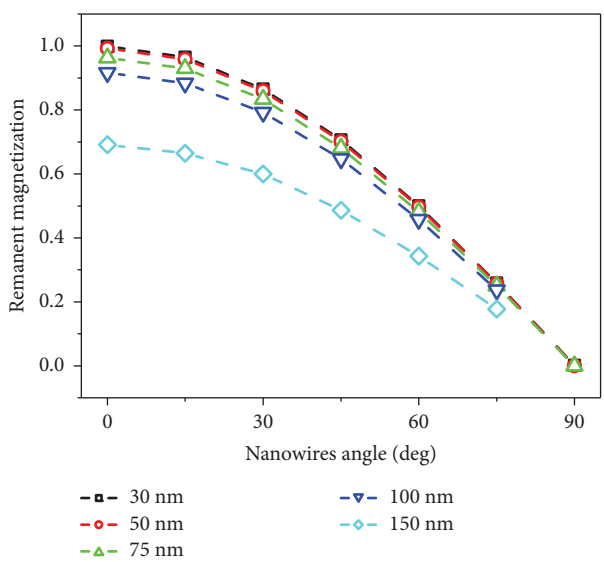

Figure 4: Remanent magnetization against permalloy wire angle for five different thicknesses as designated in the figure. The dashed lines are theoretical fitting curves obtained using equation (5).

nanowires T was analyzed in detail elsewhere [43, 44], and it was attributed to the formation of multidomain structures or moment rotations within the sample due to the effect of the shape anisotropy and demagnetizing field, which increases with increasing nanowire thickness.

According to the theoretical calculations and micromagnetic analysis performed in the literature, there are various distinct classical mechanisms that are able to describe the reversal processes in such nano-objects, including buckling and fanning models, as well as coherent rotation of the Stoner–Wohlfarth and incoherent rotation of curling models of domain reversal. Detailed theoretical descriptions of these classical models can be found elsewhere [28, 29, 66–71].

Thus, to understand the mechanism responsible for the angular dependence of the nanowires investigated here, it should first be noted that since buckling reversal is expected to occur when the nanowires T are comparable to the exchange length (reduced thickness around unity) [66, 70], buckling may be excluded from the applicability on such

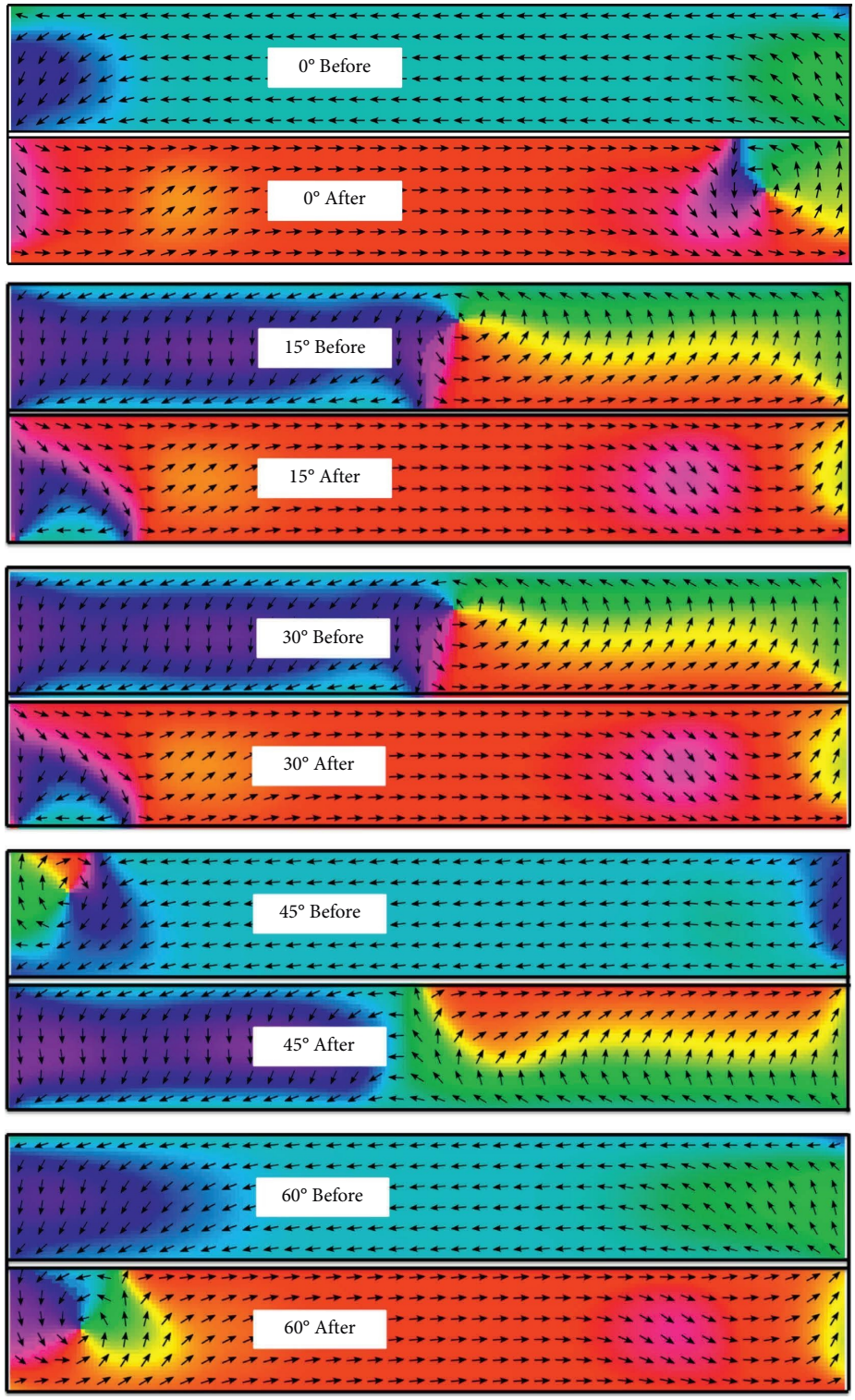

Figure 5: Snapshots of magnetic moment distributions along the center of the permalloy wires of 150 nm thickness obtained from energy-minimized states at two different field steps during the switching field and at various angles of simulations, as indicated in the figures. The color variation represents the *x-y* and *x-z* angles of the magnetic spin.

nanowires. On the other hand, the aspect ratio and shape of such nanowires are far from being a chain of spheres, which would reverse as in the fanning model. Therefore, the angular dependence of the switching fields is likely to be the consequence of a coherent (thin wires ≤ 30 nm) and an incoherent rotational process (thick wires ≥ 50 nm) following the Stoner–Wohlfarth and curling models of domain reversal, respectively. Accordingly, all the switching

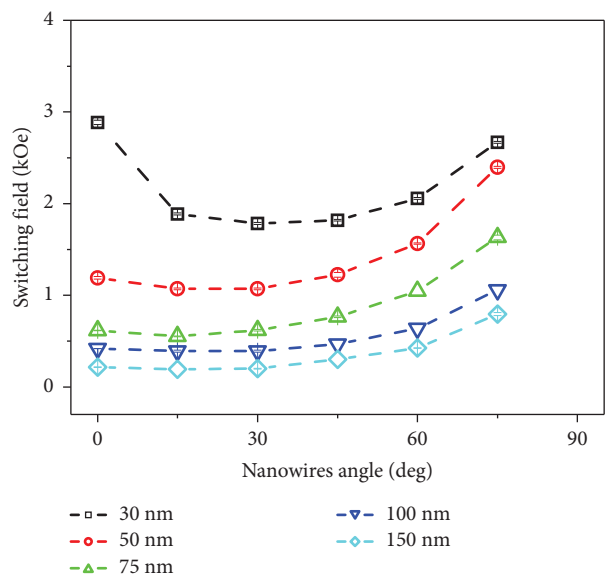

FIGURE 6: Switching field as a function of the angle of permalloy wires for different T of nanowires, as shown in the figure. The dashed lines provide a guide for the eye.

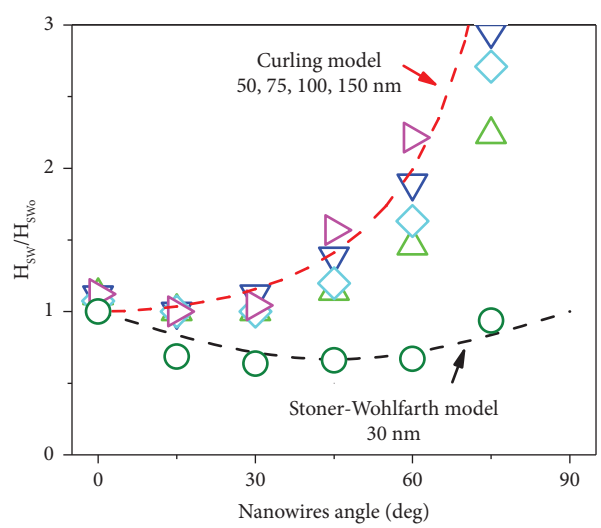

FIGURE 7: Normalized switching field as a function of the angle of permalloy wires with various T as specified in the figure. The dashed curves represent the theoretical fit of the uniform and nonuniform models of domain wall reversal as specified in the figure.

fields extracted from the simulation hysteresis loops were matched with the theoretical calculations of the Stoner–Wohlfarth (for nanowires of $T \leq 30$ nm) and curling models (for nanowires of $T \geq 50$ nm) after normalizing the switching fields, H_{sw}, to the minimum values using the equations (6)–(10) presented in the methodology section and are shown in Figure 7. Excellent agreement was seen at all angles of discussion, proposing that these classical models of domain reversal are a rational analytical illustration of the magnetization reversal in such permalloy wires, in spite of the micromagnetic spin configurations and the loops shape, which were established earlier, demonstrating the complexity of the spin structure and the appearance of different switching events through the magnetization reversal in relatively thick permalloy nanowires. To understand this behavior in more details, similar investigations are required using wires with T between 100 nm and 300 nm.

4. Conclusions

Micromagnetic simulations were performed using the OOMMF platform to explore the magnetic properties of $Ni_{81}Fe_{19}$ nanostructures with various T up to 150 nm and an identical stretch of 1 μm.

The highest (lowest) remanent M_β was found when the external magnetic field was applied parallel (normal) to the wire's long axis, demonstrating the dominance of

shape anisotropy on the behavior. This result was in full agreement with the mathematical representations performed here.

The shape of the hysteresis loops of relatively thick (150 nm) wire was complicated, displaying various switching events by increasing the wire's angle.

The angular dependence revealed that nanowires ≤30 nm thicknesses behaved differently from nanowires ≥50 nm. This result was in excellent agreement with the calculations performed here theoretically and with the results stated experimentally in the literature using other characterization methods and other compositions of ferromagnetic nanowires. The angular dependence of the switching field was also in full agreement with the classical models of reversal. This agreement indicates that these models are a rational and methodical demonstration of the magnetization reversal in such wires, although the micromagnetic spin structures of relatively thick nanowires showed the complexity of the magnetic moment structure before and after the reversal.

Data Availability

The hysteresis loops, snapshots, and angular dependence of switching field and remanence magnetization used to support the findings of this study are included within the article. Further details are available from the corresponding author.

Disclosure

A part of this research was included in the author's PhD thesis (Experimental and Micromagnetic Study of Magnetization Behavior in Isolated Ferromagnetic Nanowires).

Conflicts of Interest

The author would like to declare that there are no conflicts of interest regarding the publication of this paper.

Acknowledgments

The author would like to thank Prof. Dr. Del Atkinson at the Physics Department, Durham University, UK, for his assistance throughout this work. The author would also like to thank Dr. David Burn, UK, for his appreciated assistance throughout this work. This research is personally funded and the author is responsible for the publication fees.

References

[1] S.-W. Lee, M.-C. Jeong, J.-M. Myoung, G.-S. Chae, and I.-J. Chung, "Magnetic alignment of ZnO nanowires for optoelectronic device applications," *Applied Physics Letters*, vol. 90, no. 13, Article ID 133115, 2007.

[2] E. Cisternas, J. Faúndez, and E. E. Vogel, "Stabilization mechanisms for information stored in magnetic nanowire arrays," *Journal of Magnetism and Magnetic Materials*, vol. 426, p. 588, 2017.

[3] A. Kunz, S. C. Reiff, J. D. Priem, and E. W. Rentsch, "Controlling individual domain walls in ferromagnetic nanowires for memory and sensor applications," *International Conference on Electromagnetics in Advanced Applications*, vol. 248, 2010.

[4] J. C. Lodder, "Methods for preparing patterned media for high-density recording," *Journal of Magnetism and Magnetic Materials*, vol. 1692, pp. 272–276, 2004.

[5] D. Atkinson, D. S. Eastwood, and L. K. Bogart, "Controlling domain wall pinning in planar nanowires by selecting domain wall type and its application in a memory concept," *Applied Physics Letters*, vol. 92, no. 2, Article ID 022510, 2008.

[6] A. Hultgren, M. Tanase, C. S. Chen, G. J. Meyer, and D. H. Reich, "Cell manipulation using magnetic nanowires," *Journal of Applied Physics*, vol. 93, no. 10, p. 7554, 2003.

[7] W. Andra, U. Hafeli, R. Hergt, and R. Misri, "Handbook of magnetism and advanced magnetic materials: application of magnetic particles in medicine and biology," *Novel Materials*, John Wiley & Sons Ltd, Hoboken, NJ, USA, 2007.

[8] B. Koopmans, M. van Kampen, J. T. Kohlhepp, and W. J. M. de Jonge, "Ultrafastmagneto-optics in nickel: magnetism or optics?" *Physical Review Letters*, vol. 85, no. 4, pp. 844–847, 2000.

[9] J. Hohlfeld, T. Gerrits, M. Bilderbeek, T. Rasing, H. Awano, and N. Ohta, "Fast magnetization reversal of GdFeCo induced by femtosecond laser pulses," *Physical Review B: Condensed Matter*, vol. 65, no. 1, Article ID 012413, 2001.

[10] C. Stamm, T. Kachel, N. Pontius et al., "Femtosecond modification of electron localization and transfer of angular momentum in nickel," *Nature Materials*, vol. 6, no. 10, pp. 740–743, 2007.

[11] M. Vomir, L. H. F. Andrade, L. Guidoni, and E. Beaurepaire, "Real space trajectory of the ultrafast magnetization dynamics in ferromagnetic metals," *Physical Review Letters*, vol. 94, no. 23, Article ID 237601, 2005.

[12] C. Y. Hsu, A. M. Rheima, M. M. Kadhim, U. S. Altimari, and A. H. Dawood, "Nanowires properties and applications: a review study," *South African Journal of Chemical Engineering*, vol. 46, 2023.

[13] D. Jiles, *Introduction to Magnetism and Magnetic Materials*, Chapman and Hall/CRC, New York, NY, USA, 1998.

[14] B. D. Cullity and C. D. Graham, *Introduction to Magnetic Materials*, John Wiley & Sons Inc, NJ, USA, 2009.

[15] S. Chikazumi, *Physics of Ferromagnetism*, Clarendon Press, Oxford, UK, 1997.

[16] R. Skomski, "Topical review: nanomagnetics," *Journal of Physics: Condensed Matter*, vol. 15, 2003.

[17] F. Nasirpouri, "Template electrodeposition of magnetic nanowire arrays," *Trans world Res. Net.*, vol. 661, no. 37, 2007.

[18] J. M. D. Coey and G. Hinds, *Magnetic electrodeposition J. Alloys and Compounds*, vol. 326, no. 1-2, pp. 238–245, 2001.

[19] K. Nielsch and B. J. H. Stadler, "Handbook of magnetism and advanced magnetic materials: template-based synthesis and characterization of high-density ferromagnetic nanowire arrays," *Novel Materials*, John Wiley & Sons Ltd, Hoboken, NJ, USA, 2007.

[20] E. G. Possin, "A method for forming very small diameter wires," *Review of Scientific Instruments*, vol. 41, p. 772, 1970.

[21] L. Sun, Y. Hao, C. L. Chien, and P. C. Searson, "Tuning the properties of magnetic nanowires," *IBM Journal of Research and Development*, vol. 49, no. 1, p. 79, 2005.

[22] B. Das, C. Ting-Chieh, S. Deng-Shiang, L. Horng, and J.-C. Wu, "Diferential domain wall propagation in Y-shaped permalloy nanowire devices," *World science*, vol. 6, no. 1, Article ID 1650006, 2016.

[23] C. Ting-Chieh, K. Cheng-Yi, and A. K. Mishra, "Das Bipul, Wu Jong-Ching Magnetic domain wall motion in notch

patterned permalloy nanowire devices," *Physica B: Condensed Matter*, vol. 476, p. 161, 2015.

[24] D. A. Alwood, G. Xiong, C. C. Faulkner, D. Atkinson, D. Petit, and R. P. Cowburn, "Magnetic domain-wall logic," *Science*, vol. 309, p. 1688, 2005.

[25] E. Nikulina, O. Idigoras, P. Vavassori, A. Chuvilin, and A. Berger, "Magneto-optical magnetometry of individual 30 nm cobalt nanowires grown by electron beam induced deposition," *Applied Physics Letters*, vol. 100, Article ID 142401, 2012.

[26] A. Fernández-Pacheco, D. Teresa, A. Szkudlarek et al., "Magnetization reversal in individual cobalt micro-and nanowires grown by focused-electron-beam-induced-deposition," *Nanotechnology*, vol. 20, no. 47, Article ID 475704, 2009.

[27] A. Fernandez Pacheco, D. Teresa, R. Cordoba, and M. R. Ibarra, "Magnetotransport properties of high-quality cobalt nanowires grown by focused-electron-beam-induced deposition," *Journal of Physics D Applied Physics*, vol. 42, p. 5, 2008.

[28] A. B. Oliveira and A. Azevedo, "Magnetization reversal in single ferromagnetic rectangular nanowires," *Journal of Physics: Conf. Series*, vol. 200, no. 7, Article ID 072023, 2010.

[29] A. B. Oliveira, S. M. Rezende, and A. Azevedo, "Magnetization reversal in permalloy ferromagnetic nanowires investigated with magnetoresistance measurements," *Physical Review B: Condensed Matter*, vol. 78, no. 2, Article ID 024423, 2008.

[30] Y. Rheem, B. B.-Y. Yoo, W. P. Beyermann, and N. V. Myung, "Magnetotransport studies of a single nickel nanowire," *Nanotechnology*, vol. 18, Article ID 015202, 2007.

[31] Y. Rheem, B.-Y. Yoo, B. K. Koo, W. P. Beyermann, and N. V. Myung, "Synthesis and magnetotransport studies of single nickel-rich NiFe nanowire," *Journal of Physics D Applied Physics*, vol. 40, no. 23, p. 7267, 2007.

[32] Y. Rheem, B.-Y. Yoo, W. P. Beyermann, and N. V. Myung, "Magneto-transport studies of single ferromagnetic nanowire," *Physica Status Solidi*, vol. 204, no. 12, p. 4004, 2007.

[33] Y. Rheem, B.-Y. Yoo, W. P. Beyermann, and N. V. Myung, "Electro-and magneto-transport properties of a single CoNi nanowire," *Nanotechnology*, vol. 18, no. 12, Article ID 125204, 2007.

[34] M. S. Sultan, "Electro and magneto transport behaviour of template released isolated ferromagnetic nanowires," *IEEE Transactions on Magnetics*, vol. 53, no. 12, p. 1, 2017.

[35] W. Wernsdorfer, B. Doudin, D. Mailly et al., "Nucleation of magnetization reversal in individual nanosized nickel wires," *Physical Review Letters*, vol. 77, no. 9, p. 1873, 1996.

[36] W. Wernsdorfer, G. Cedex, and B. Barbar, "Measurements of magnetization switching in individual nickel nanowires," *Physical Review B: Condensed Matter*, vol. 55, no. 17, p. 552, 1997.

[37] M. S. Sultan, B. Das, P. Sen, K. Mandal, and D. Atkinson, "Template released ferromagnetic nanowires: morphology and magnetic properties," *J. Spintron. Magn. Nanomater.*, vol. 1, 2012.

[38] N. Lupu, M. Lostun, and H. Chiriac, "Surface magnetization processes in soft magnetic nanowires," *Journal of Applied Physics*, vol. 107, no. 9, Article ID 09E315, 2010.

[39] M. Ester, C. Bran, and M. Vázquez, "Vortex domain wall propagation in periodically modulated diameter FeCoCu nanowire as determined by the magneto optical Kerr effect," *Nanotechnology*, vol. 26, Article ID 461001, 2015.

[40] M. S. Sultan, "Surface and bulk magnetisation behavior of isolated ferromagnetic NiFe nanowires World Academy of Science, Engineering and Technology," *International Science Index, Physical and Mathematical Sciences*, vol. 12, no. 5, p. 829, 2018.

[41] M. S. Sultan, "Angular dependence of switching behaviour in template released isolated NiFe nanowires," *Physics Letters A*, vol. 381, no. 46, p. 3896, 2017.

[42] M. S. Sultan, "Surface morphology and magnetic properties of isolated cylindrical nickel nanowires," *American Journal of Nanosciences*, vol. 30, p. 3, 2017.

[43] M. S. Sultan and D. Atkinson, "Aspect-ratio dependence of magnetization reversal in cylindrical ferromagnetic nanowires," *Materials Research Express*, vol. 3, Article ID 056104, 2016.

[44] N. Han, G. Guo, L. Zhang, G. Zhang, and W. Song, "Magnetization reversal for Ni nanowires studied by micromagnetic simulations," *Journal of Materials Science & Technology*, vol. 25, no. 2, p. 151, 2009.

[45] N. Han, G. Guo, Z. Guang-fu, S. Wen-bing, Gao-fu, and Men, "Domain wall structure transition during magnetization reversal process in magnetic nanowires Trans," *Nonferrous Met. Soc. China*, vol. 17, Article ID 60571043, p. 1034, 2007.

[46] R. Hertel, "Micromagnetic simulations of magnetostatically coupled nickel nanowires," *Journal of Applied Physics*, vol. 90, no. 11, p. 5752, 2001.

[47] J.-H. Gao, D.-L. Sun, Q.-F. Zhan, W. He, and Z.-H. Cheng, "Magnetization reversal process and magnetic relaxation of self-assembled Fe_3Pt nanowire arrays with different diameters: experiment and micromagnetic simulations," *Physical Review B: Condensed Matter*, vol. 75, no. 6, Article ID 064421, 2007.

[48] P. Yu, M. Ivanov, and O. Vazquezl, "Chubykalo-Fesenko Magnetic reversal modes in cylindrical nanowires," *Journal of Physics D Applied Physics*, vol. 46, Article ID 485001, p. 11, 2013.

[49] R. Hertel and J. Kirschner, "Magnetization reversal dynamics in nickel nanowires," *Physica B: Condensed Matter*, vol. 343, no. 1-4, p. 206, 2004.

[50] H. Forster, T. Schrefl, W. Scholz, D. Suess, V. Tsiantos, and J. Fidler, "Micromagnetic simulation of domain wall motion in magnetic nano-wires," *Journal of Magnetism and Magnetic Materials*, vol. 249, no. 1-2, p. 181, 2002.

[51] R. Hertel, "Computational micromagnetism of magnetization processes in nickel nanowires," *Journal of Magnetism and Magnetic Materials*, vol. 249, no. 1-2, p. 251, 2002.

[52] K. M. Lebecki, "Modelling of magnetization reversal for long ferromagnetic nanotubes," *Materials Science-Poland*, vol. 26, no. 4, 2008.

[53] A. P. Chen, J. Gonzalez, and K. Y. Guslienko, "Domain walls confined in magnetic nanotubes with uniaxial anisotropy," *Journal of Magnetism and Magnetic Materials*, vol. 324, no. 22, p. 3912, 2012.

[54] S. Allende, J. Escrig, D. Altbir, E. Salcedo, and M. Bahiana, "Angular dependence of the transverse and vortex modes in magnetic nanotubes," *The European Physical Journal B*, vol. 66, no. 1, p. 37, 2008.

[55] P. M. Paulus, F. Luis, M. Kro, G. Schmid, and L. J. D. Jongh, "Low-temperature study of the magnetization reversal and magnetic anisotropy of Fe, Ni and Co nanowires," *Journal of Magnetism and Magnetic Materials*, vol. 224, 2001.

[56] M. J. Donahue and D. G. Porter, "OOMMF user's guide, version 1.0," *NISTIR 6376*, National Institute of Standards & Technology, Gaithersburg, MD, USA, 1999.

[57] D. Kumar and A. O. Adeyeye, "Techniques in micromagnetic simulation and analysis," *Journal of Physics D Applied Physics*, vol. 50, Article ID 343001, p. 19, 2017.

[58] J. Fidler and T. Schrefl, "Micromagnetic modelling-the current state of the art," *Journal of Physics D Applied Physics*, vol. 33, pp. R135–R156, 2000.

[59] J. Fidler, P. Speckmayer, T. Schrefl, and D. Suess, "Numerical micromagnetics of an assembly of (Fe, Co) Pt nanoparticles," *Journal of Applied Physics*, vol. 97, no. 10, Article ID 10E508, 2005.

[60] S. Sundara Mahalingam, B. V. Manikandan, and S. Arockiaraj, "Review micromagnetic simulation using OOMMF and experimental investigations on nano composite," *Magnets IOP Conf. Series: Journal of Physics: Conference Series*, vol. 1172, Article ID 012070, 2019.

[61] K. J. Kirk and J. N. Chapman, "CDW Lorentz microscopy of small magnetic structures," *Journal Applied Physics*, vol. 85, no. 8, p. 5237, 1999.

[62] S. Gavin, "Definition of magnetic exchange Length," *IEEE Transactions on Magnetics*, vol. 49, p. 8, 2013.

[63] M. S. Sultan, *Experimental and micromagnetic study of magnetisation behaviour in isolated ferromagnetic nanowires*, Ph.D. thesis submitted to Durham University, Durham University, Durham, England, 2013.

[64] K. Moon, J. Lee, M. Jung, K. Shin, and S. Choe, "Incoherent domain configuration along wire width in permalloy nanowires," *IEEE Transactions on Magnetics*, vol. 45, no. 6, p. 2485, 2009.

[65] Mmf, "Software," 2012, https://math.nist.gov/oommf/software.html.

[66] A. Aharoni, "Magnetization buckling in a prolate spheroid," *Journal of Applied Physics*, vol. 60, no. 3, p. 1118, 1986.

[67] A. Aharoni, "Curling reversal mode in nonellipsoidal ferromagnetic particles," *Journal of Applied Physics*, vol. 86, no. 2, p. 1041, 1999.

[68] A. Aharoni and S. Shtrikman, "Magnetization curve of the infinite cylinder," *Physics Reviews*, vol. 109, no. 5, p. 1522, 1958.

[69] E. C. Stoner and E. P. Wohlfarth, "A mechanism of magnetic hysteresis in heterogeneous alloys," *Philosophical Transactions of the Royal Society of London-A*, vol. 240, no. 826, p. 599, 1948.

[70] A. Aharoni, *Introduction to the Theory of Ferromagnetism*, Clarendon Press Inc, Oxford, UK, 1998.

[71] M. Volmer and J. Neamtu, "Simulation of magnetisation curves in magnetic thin films using Stoner-Wohlfarth model," *Romanian Reports in Physics*, vol. 56, no. 3, p. 367, 2004.

[72] J. M. Porro, A. Villar, C. Redondo, and A. Natalia, "Competition of magnetic anisotropies in permalloy antidot lattices," *Magneto chemistry*, vol. 8, p. 5, 2022.